SCIENTIFIC CULTURE

www.sci-cult.com

SCIENTIFIC CULTURE, Vol. 12, No. 2.1, (2026), pp. 3897-3915
Open Access. Online & Print

DOI: 10.5281/zenodo. 18866820

EFFECT OF TEMPERATURE ON THE STRUCTURE, MORPHOLOGY, TEXTURE AND ADSORBENT PROPERTIES OF A BIOGENIC SILICA

Grey Cecilia Castellar Ortega[1], Yazmín Yaneth Agámez Pertuz[2], Nubia Edith Céspedes Prieto[3], Eduard Ricardo Romero Malagón[4], Luis Carlos Moreno Aldana[5], Jesús Sigifredo Valencia Ríos[6]

[1]Universidad Autónoma del Caribe, Grupo de Investigación Interdisciplinario de Ciencias Básicas, Barranquilla, Colombia, Universidad Nacional de Colombia, Laboratorio de Catálisis Heterogénea, Aplicaciones Fisicoquímicas del Estado Sólido, Departamento de Química, Facultad de Ciencias, Bogotá D.C., Colombia
[2]Universidad Nacional de Colombia, Laboratorio de Investigación en Combustibles y Energía, Departamento de Química, Facultad de Ciencias, Bogotá D.C., Colombia
[3]Escuela de Ingenieros Militares, Ejército Nacional de Colombia, Bogotá D.C., Colombia
4Universidad Nacional de Colombia, Laboratorio de Investigación en Combustibles y Energía, Departamento de Química, Facultad de Ciencias, Bogotá D.C., Colombia
5Universidad Nacional de Colombia, Laboratorio de Catálisis Heterogénea, Aplicaciones Fisicoquímicas del Estado Sólido, Departamento de Química, Facultad de Ciencias, Bogotá D.C., Colombia, Universidad Nacional de Colombia, Laboratorio de Investigación en Combustibles y Energía, Departamento de Química, Facultad de Ciencias, Bogotá D.C., Colombia
6Universidad Nacional de Colombia, Laboratorio de Catálisis Heterogénea, Aplicaciones Fisicoquímicas del Estado Sólido, Departamento de Química, Facultad de Ciencias, Bogotá D.C., Colombia

Received: 24/12/2025
Accepted: 16/02/2026

ABSTRACT

Among natural ceramic materials, diatomaceous earth is of special interest due to its low toxicity, high porosity and permeability, with good mechanical and chemical stability, which have allowed it to be used as an adsorbent and filter bed, among other applications. In this research, the effect of the calcination temperature between 200 and 1000 °C, for 6 h in an air atmosphere, on the crystalline phases, morphology, texture and adsorbent properties, in the removal of methylene blue dye (MA), from a representative sample of biogenic silica from the municipality of Chivatá (Boyacá) in Colombia, was evaluated. The results of the adsorption-desorption isotherms of N2 at 77 K correspond to type IV, typical of mesoporous materials, with surface area development from 45.2 m2g-1 to 53.8 m2 g-1 at 500 °C. X-ray diffraction analysis indicates that it is an amorphous silica with the presence of crystalline phases such as quartz, kaolinite and muscovite. The reflections of the quartz are maintained during calcination, while the reflections of the clays disappear. Micrographs show the predominance of porous cylindrical frustules that are preserved even after calcination. The maximum adsorption capacity of the AM dye was 58.5; 51.5 and 6.81 mg g-1 for crude diatomaceous earth, and calcined at 500 and 1000 °C, respectively; with a satisfactory fit of the experimental data to the Langmuir

isotherm model. The Bed Height Service Time (BDST) model applied to the column study fits satisfactorily to all bed heights in the column. In conclusion, the persistence of mesoporosity and the conservation of the fustules show the high thermal stability of the diatomaceous earth, but calcination decreases its adsorbent capacity in the removal of the methylene blue dye in aqueous solution.

KEYWORDS: Diatomaceous Earth, Calcination, Textural Properties, Morphology, Methylene Blue, Adsorption Isotherms, Rupture Curves.

1. INTRODUCTION

Diatomaceous earth is an amorphous hydrated natural silica (SiO2. nH2O) of sedimentary origin, consisting mainly of the accumulation of the fossilized remains of diatoms, microscopic unicellular algae found in almost all aquatic environments [1, 2, 3]. These microorganisms use their cell wall to manufacture silica mineral tissue known as a sprustule [4], through the filtration of silicon mainly in the form of Si(OH)4 silicic acid, which polymerizes and forms an amorphous solid [5]. The morphogenesis of biosilica occurs within the cell, in organelles called "silica disposal vesicles" [4]. These vesicles contain many organic macromolecules that manage the formation of silica and also function as a template that regulates the growth of the frústule and helps create indentations and holes [6]. The death of large quantities of diatoms in certain regions and the subsequent sedimentation of the minerals present in the cell wall, millions of years ago, formed the deposits of diatomaceous earths [7].

Diatomaceous earth is characterized by being an easily crushed ceramic material, with high porosity and permeability, low density and thermal conductivity, and by presenting good chemical and mechanical stability; its relatively low cost and abundance [2, 3, 7-9], have allowed its use in various applications, such as in the purification and supply of drinking water [7], in the removal of metal ions and organic contaminants in aqueous media [1, 9, 10], as a filter bed in beverage clarification [11], as a catalytic support in oil transesterification reactions [12-15]. It is also used in photocatalysis for environmental remediation purposes [16, 17], in the health area as a drug delivery system [4, 18], and as a ceramic material in the construction industry [19-22].

For these applications, the use of diatomaceous earth requires cleaning the siliceous structure, that is, removing organic matter, carbonates, iron oxide, oxides of alkali and alkaline earth metals, among others, considered contaminants. Chemical treatment is a common method used to purify diatomaceous earth and modify its surface properties. Strong mineral acids are generally used [23, 24], but their untreated effluents pollute the environment a lot [25, 26]. Heat treatment is another method used to remove physically adsorbed water and dehydroxylate the silanol groups [27]. In addition, calcination causes the decomposition of carbonates into CO2 and H2O, and the removal of the organic matter present.

The evaluation of the modifications of texture, crystallinity and morphology, which occur during the heat treatment of a sample of diatomaceous earth from the municipality of Chivatá (Boyacá), Colombia, is of great importance, since it allows to guide its potential use and application in various technological processes, as is the case of intervening as supports in the preparation of oxides of alkaline earth metals as heterogeneous catalysts for alkolysis reactions of triacylglycerides. In this sense, the objective of this research is to evaluate the effect of the calcination temperature between 200 and 1000 °C, on the crystal structure, texture (surface area and porosity), thermal stability, morphology and adsorption capacity against the removal of methylene blue in aqueous solution. The results of the batch adsorption studies conform to the models of the Langmuir and Freundlich isotherms; fixed-bed column removal experiments are compatible with the service-time model proposed by Bohart and Adams.

2. MATERIALS AND METHODS

2.1. Source of the Diatomaceous Earth and Preparation of the Sample

The diatomaceous earth comes from the deposit called El Pino located in the municipality of Chivatá, in the central-eastern region of the department of Boyacá (Colombia). The sample was mechanically crushed to a size of less than 180 µm (US Standard 80 mesh), then carefully mixed to ensure homogeneity, and a representative portion was selected by quartering. Finally, it was washed with distilled water to remove fine material and other impurities, and dried at 105 °C for 12 h.

2.2. Thermal Modification of the Diatomaceous Earth

Crude diatomaceous earth (Td) was calcined at temperatures between 200 and 1000 °C for 6 h in an air atmosphere at a heating rate of 10 °C min-1, in a Thermo Scientific–F6018 muffle. Raw and treated solids are identified by the TX nomenclature, where X represents the calcination temperature in °C.

2.3. Characterization of Raw and Calcined Diatomaceous Earth

The analyses of the crystal structure of the crude and calcined diatomaceous earth were performed by X-ray diffraction (XRD) in a PANanlytical X'pert Pro equipment with a wavelength radiation Kα = 1.540598 Å, in the range between 10 and 80° at a speed of 0.02° s-1, the acceleration voltage was fixed at 45 kV and the tube current at 40 mA. The functional groups were analyzed by Fourier transform infrared spectrophotometry (IRTF) in the

range between 4000 and 400 cm-1, by the KBr pill method, in a Thermo Fisher Scientific Nicolet iS 10 spectrometer. The morphology was evaluated by scanning electron microscopy (SEM) in a Tescan Vega3 SBU equipment. Textural properties were determined from the adsorption isotherm of N2 at 77 K, in a Micromeritics Gemini IV analyzer. Finally, a thermogravimetric analysis was performed on the raw diatomaceous earth in a TGA/DSC 1 STARe equipment (Mettler Toledo), with a flow of 10 cm3 min-1 of nitrogen, heating rate of 10.0 °C min-1 in the temperature range between 25 and 1000 °C using an alumina crucible, and 5.1069 mg of sample.

2.4. Adsorption Study

2.4.1. Adsorbate

The basic dye methylene blue (C16H18ClN3S.3H2O) of high purity, brand Sigma Aldrich, was used as absorbable, due to the good adsorption results reported in other studies with diatomaceous earth [28-30].

2.4.2. Batch Studies

Initially, a "stock" solution of the AM dye was prepared, dissolving the necessary amount in distilled water. From this solution, dilutions between 20.0 and 200.0 mg dm-3 were prepared. 50 mg of diatomaceous earth was supplemented with 20 cm3 of each dilution separately at 23 °C, which was placed in a horizontal agitator at 120 rpm for 2 h. After separation by centrifugation, an aliquot of the supernatant was taken and its absorbance at 664.5 nm obtained by pre-scanning was determined in a LabScient 1150 UV VIS spectrophotometer. The same procedure was performed with the calcined diatomaceous earth at 500 and 1000 °C, identified as CQX and CMX respectively, where X represents the concentration of the AM dye. 3 replicates were performed for a total of 63 tests. The Td200, CQ200 and CM200 samples underwent Fourier transform infrared spectrophotometry (IRTF) and their textural properties were determined, with the same equipment and conditions described in section 2.3. The experimental results were adjusted to two models of adsorption isotherms: Langmuir and Freundlich. Equations 1 and 2 express the linear equation of both models, respectively [31].

$$\frac{C_e}{q_e} = \frac{C_e}{q_{max}} + \frac{1}{q_{max} K_L} \quad (1)$$

$$\ln q_e = \ln K_F + \frac{1}{n} \ln C_e \quad (2)$$

Where is the concentration at equilibrium of the adsorbate (mg dm-3C_e), and are the adsorption capacity at an equilibrium concentration and the maximum respectively (mg $q_e q_{max}$ g-1), is the Langmuir constant (dm K_L 3 mg-1), is the Freundlich constant at ((mg K_F g-1) (dm3 mg-1)1/n) and n It is a constant related to the affinity between the adsorbent and the adsorbate.

2.4.3. Column Studies

The experimental setup used for this study consisted of a glass column 18 cm high and 5 mm internal diameter, two glass vessels, one to contain the AM dye solution, before entering the column and another at the exit of the column, and a Spectrochem Instruments peristaltic pump. The experiments were performed at an initial concentration of 20.0 mg dm-3, with three bed heights (1.0, 1.5 and 2.0 cm) and a volumetric flow of 0.5 cm3 min-1 at 23 °C. At regular intervals of time, aliquots of the fluid at the exit of the bed were taken with a syringe, centrifuged, and absorbance measured using the same method described in section 2.4.2. The adsorbents selected were raw and calcined diatomaceous earth at 500 °C.

The amount of methylene blue dye removed per gram of adsorbent at the breaking point, (mg q_b g-1), was calculated from equation 3.

$$q_b = \frac{Q_v t_{10\%} C_o}{1.000m} \quad (3)$$

Where is the breakdown time (min), is the initial concentration or entry to the column (mg dm-3 $t_{10\%} C_o$), is the volumetric flow (cmQ_v 3 min-1), is the mass of adsorbent (g) and the value of 1,000 corresponds to a conversion factor. m

The experimental results were adjusted to the model of the service time of the height of a bed (BDST). This model, proposed by Bohart and Adams in 1920, establishes the relationship between bed height, , and column service time, . Equation 4 shows the initial expression proposed by Bohart and Adams [32]. Zt

$$ln\left(\frac{C_o}{C} - 1\right) = ln\left(e^{\left(\frac{KN_oZ}{U} - 1\right)}\right) - KC_o t \quad (4)$$

If it is admitted that >>1, then the term $e^{\left(KN_o\frac{Z}{U}\right)} ln(e^{\left(KN_o\frac{Z}{U}\right)} - 1)$ can approximate , resulting in a new equation (5) $lne^{\left(KN_o\frac{Z}{U}\right)}$that linearly relates the height of the column bed () to the time of service [33].$Z(t)$

$$t = \frac{N_o}{C_o U} Z - \frac{1}{K C_o} \ln\left(\frac{C_o}{C} - 1\right) \quad (5)$$

Where is the service time of the column (min), is the dynamic adsorption capacity of the bed (mg dm-3t N_o), is the height of the bed (cm), is the linear flow velocity (cm Z Umin-1) defined as the quotient between the volumetric flow (cmQ_v3min-1) and the cross-sectional area of the column (cm2), is the

concentration of the adsorbable at one time (mg Ct^{dm-3}), and is the constant of adsorption rate (dm K^{3} min-1 mg-1). Equation 5 can be expressed in a simplified way as:

$$t = aZ + b \qquad (6)$$

where

$$a = \frac{N_o}{C_o U} \qquad (7)$$

y

$$b = -\frac{1}{KC_o}\ln\left(\frac{C_o}{C} - 1\right) \qquad (8)$$

3. RESULTS AND DISCUSSION

3.1. X-ray Diffraction (XRD)

Figure 1 shows the X-ray diffractogram of the raw diatomaceous earth, where the presence of opal-A with a broad signal between 19° and 34° (2θ) is observed, characteristic of these amorphous siliceous materials. The crystalline phases of the sample are the result of the presence of quartz at 20.87°, 26.68°, 36.58°, 39.52°, 42.49°, 45.74°, 50.17°, 55.14°, 60.01° and 68.23° (2θ) [34-36]; mica like Muscovite at 19.86°, 35.05° and 62.12°(2θ); kaolinite at 12.37° and 25.01° (2θ) [37]; and less intense reflections of dolomite at 31.03° (2θ) and calcite at 29.5° (2θ).

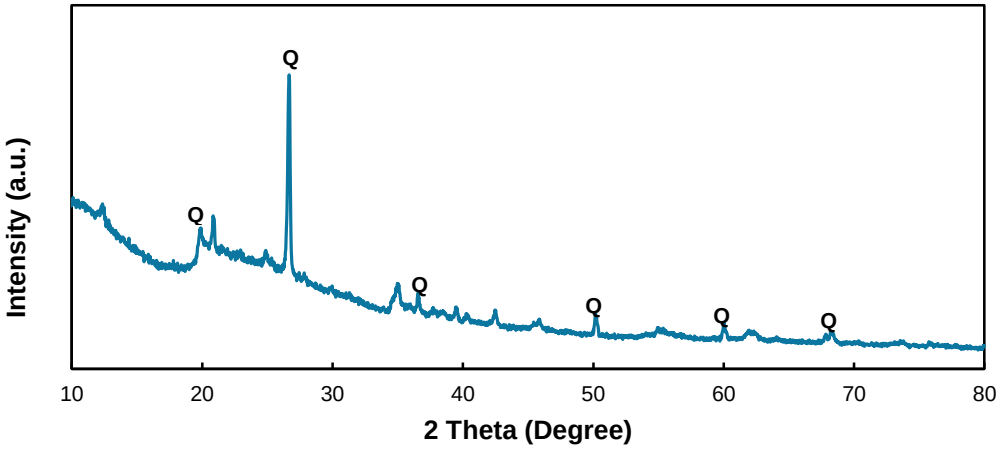

Figure 1: Diffractogram of Crude Diatomaceous Earth with the Assignment of the Peaks of Quartz (Q), Kaolinite (K), Muscovite (M), Calcite (C) and Dolomite (D).

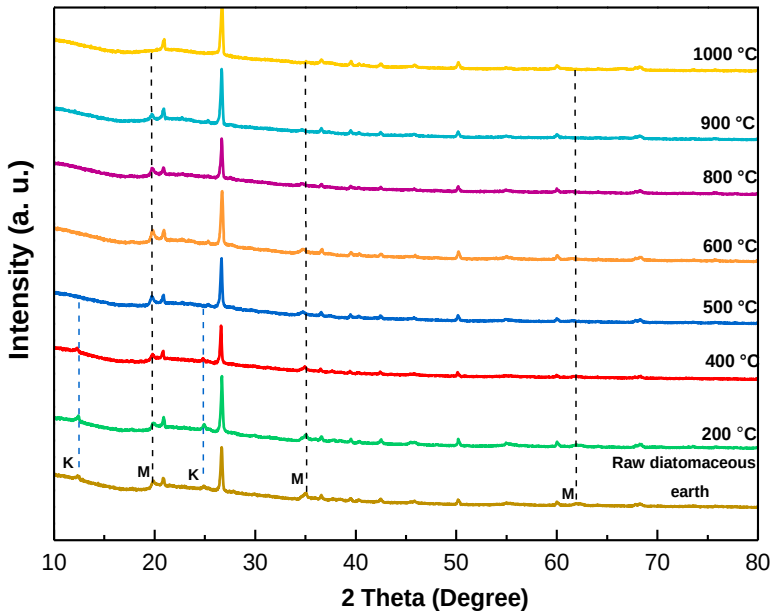

Figure 2: Diffractograms of Raw and Calcined Diatomaceous Earth at Temperatures Between 200 °C and 1000 °C, with the Assignment of the Peaks of Quartz (Q), Kaolinite (K) and Muscovite (M).

After calcination of the diatomaceous earth, several modifications in the reflections of the crystalline phases are observed (Figure 2). At 500 °C the kaolinite signals disappear mainly due to dehydroxylation reactions. According to Frost et al. (2003) and Ptàček et al. (2014) [38, 39], dehydroxylation consists of the interaction of two hydroxyl groups to form a water molecule. This causes an important structural modification mainly in the octahedral layer, where Al changes coordination from 6 to 4, while Si maintains its coordination of 4 in the tetrahedral layer, which destroys its laminar structure [39]. On the other hand, the decomposition of calcite into CaO and CO_2 is estimated to begin at approximately 500 °C and is completed at 900 °C. In this same temperature range, dolomite initially breaks down into $CaCO_3$, MgO, and CO_2, and continues with the calcite reaction [40]. Finally, the Muscovite phase decomposes in the temperature range between 900 and 1000 °C [35]. The signals for opal-A and quartz remain unchanged after calcination.

3.2. Fourier Transform Infrared Spectrophotometry (FTIR)

In the infrared spectrum of raw diatomaceous earth, the characteristic bands of SiO2 and clays are observed, which correspond mainly to vibrations of the silicon-oxygen and silicon-oxygen-aluminum bond (Figure 3). The band most prominent for its size and elongated shape around 1093 cm^{-1} suggests asymmetrical stretching vibrations of Si-O-Si bonds due to the presence of siloxane groups [27], at 797 cm^{-1} there is a smaller band that corresponds to Si-O-Al(IV) bond vibrations (where IV indicates Al of tetrahedral coordination), and the Si-O-Al (VI) bond stretch bands (where the VI indicates octahedral coordination Al) of kaolinite at 533 cm^{-1} [41] and the O-Si-O bond at 468 cm^{-1} [1, 42]. Other less intense bands of the silanol group (Si-OH) are also observed, which correspond to stretching vibrations of the O-H bond at 3770, 3697, 3653 and 3621 cm^{-1} [1, 27], and of the Al-OH bond of kaolinite at 913 cm^{-1} [41]. Due to the presence of water adsorbed on the surface of the diatomaceous earth, a wide band associated with hydroxyl groups appears between 3500 and 3300 cm^{-1}, and another less intense one at 1616 cm^{-1} due to H-O-H angular bending vibrations [1, 43, 44]. The bands at 2920 and 2850 cm^{-1} can be attributed to C-H stretch vibrations of the CH2 and CH3 groups, due to the presence of organic matter such as humic and fulvic acids in the diatomaceous earth [44, 45]. Finally, two low-intensity bands are observed, the first, at 1380 cm^{-1} that is attributed to C-O bond vibrations of the CO32- group of the minerals calcite and dolomite [34], and the second, at 693cm^{-1} due to Si-O-Al bond vibrations, characteristic of clay minerals [46].

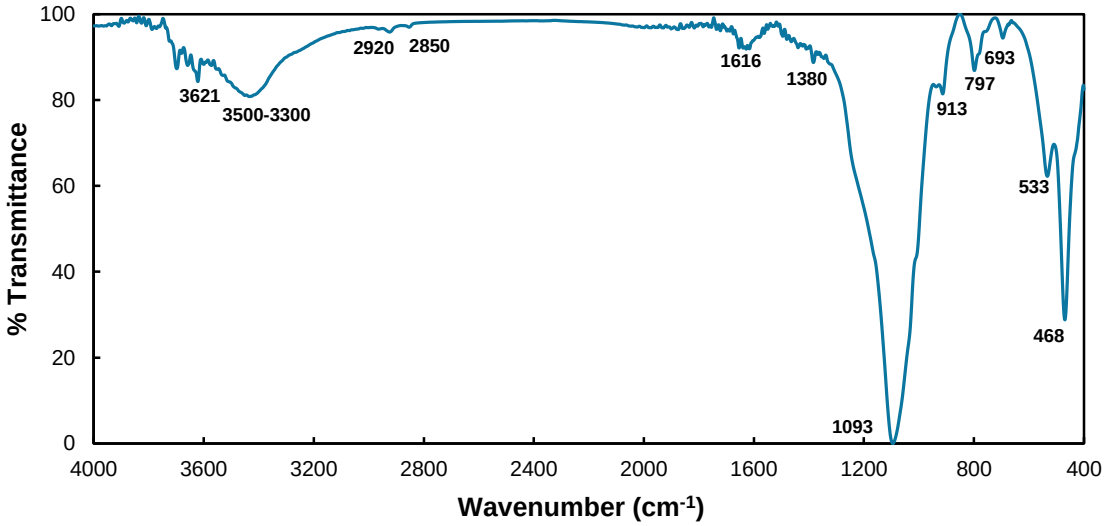

Figure 3: FTIR of Raw Diatomaceous Earth.

Changes in the IRTF caused by calcination of the diatomaceous earth are shown in Figure 4. In this figure the bands corresponding to the Si-O-Si and O-SI-O bond vibrations at 1093cm^{-1} and 468cm^{-1} respectively, associated with the presence of siloxanes in opal-A and quartz remain unchanged. At 500°C, four important changes are observed: (i) the bands related to the Si-OH bonds decrease in intensity and disappear completely at 1000°C, as a result of the sintering of the silanol groups [27]; (ii) the Al-OH and Si-O-Al(VI) bond stretch bands, respectively, at 913cm^{-1} and 533cm^{-1}, disappear,

confirming the dehydroxylation and delamination of kaolinite observed in XRD (Fig. 2), (iii) the bands associated with molecular water adsorbed at 3430 cm^{-1} and 1616 cm^{-1} decrease in intensity until they disappear completely and (iv) a new band appears at 1714 cm^{-1} due to C=O bond vibrations that suggest the presence of new CO_3^{2-} due to the thermal decomposition of the dolomite into calcite. Finally, the bands linked to the presence of organic matter in 2920 and 2850cm^{-1} decrease in intensity with increasing temperature and eventually disappear.

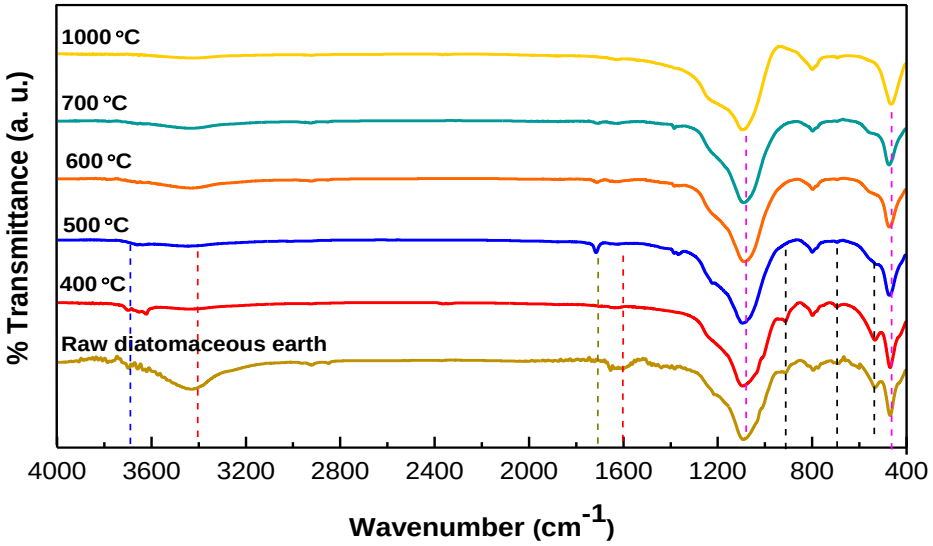

Figure 4: Comparison between the FTIR of Raw and Calcined Diatomaceous Earth.

3.3. Thermal Analysis

The behavior of the thermal analysis of raw diatomaceous earth in terms of TG is shown in Figure 5. The thermogram of the crude diatomaceous earth reveals three global processes of mass loss. The first occurs between 30 and 200°C with a percentage loss of 2.44% that is attributed to the elimination of water adsorbed and/or absorbed on the surface of the sample; This percentage is inherent to the morphology of the diatomaceous earth related to the nature, size and shape of the frustules present and the type of porosity and surface area of the sample [35, 47]. The second and third processes are widened which are observed in the interval, between 350 and 700 °C, with a total mass loss of 4.33%. At lower temperatures, the decrease in mass is associated with dehydroxylation and/or dehydration reactions by removal of structural water from the opal phase A and above 500°C it is due to the thermal decomposition of carbonates and the oxidation of organic matter [47].

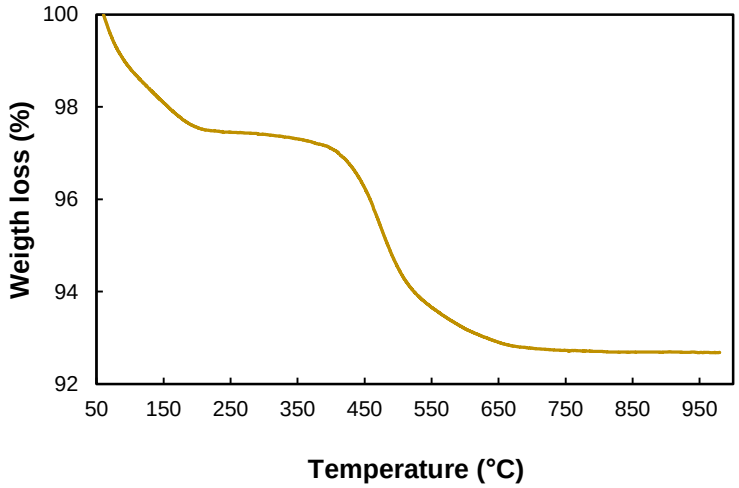

Figure 5: Thermal Analysis of Raw Diatomaceous Earth.

3.4. Textural Properties

Figure 6a shows that the adsorption-desorption isotherm of N2 at 77 K of crude diatomaceous earth is type IV with H3 hysteresis rings, according to the IUPAC classification, characteristic of mesoporous materials [48]. This type of porosity persists even after calcining at 900 °C, as capillary condensation continues. Heat treatment at 1000 °C significantly decreases the opening of the hysteresis ring, forming larger pores, but still remaining within the category of mesoporous material (Figure 6b).

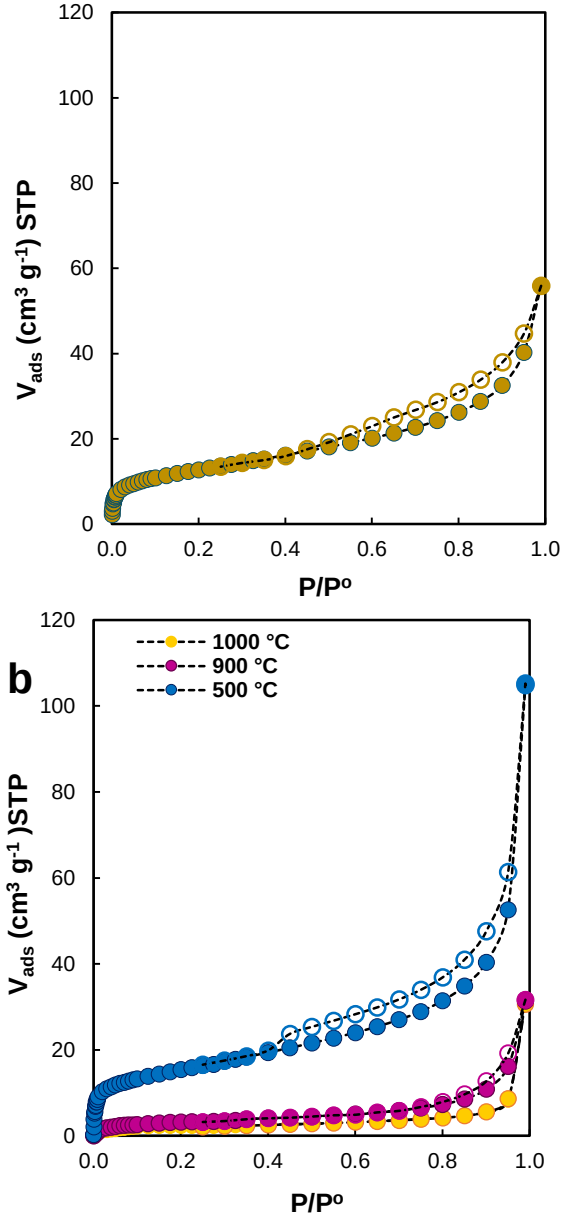

Figure 6: Adsorption-Desorption Isotherms of N□ at 77 K from Crude (a) and Calcined Diatomaceous Earth (b).

The surface area was calculated by applying the Brunauer, Emmett and Teller (BET) method with the adsorption data in the range of relative pressures between 0.04 and 0.30; the external area was calculated by applying the Jura-Harkins model and the pore size distribution using the Barrett, Joyner and Halenda (BJH) method.

Table 1: Textural Properties of Raw and Calcined Diatomaceous Earth.

Sample	Surface area SBET (m2 g^{-1})	Area External Sext (m2 g^{-1})	Micropore area Smicro (m2 g^{-1})	Average pore size (nm)
Td	45.2	41.4	3.8	7.60
T200	47.2	40.5	6.7	7.90
T400	53.2	46.1	7.1	11.5
T500	53.8	46.4	7.4	11.9
T600	52.4	48.7	3.7	9.20
T700	47.5	46.6	0.90	12.8
T800	32.6	32.0	0.60	12.7
T900	10.9	10.7	0.20	14.9
T1000	7.60	7.50	0.10	31.1

The textural properties obtained by these methodologies are presented in Table 1, from which it is inferred that the greatest adsorption of N2 occurs in the mesoporous part of the solids, with the external area being the one that mainly contributes to the total area (SBET). The contribution of micropores is lower, but these are the ones that are most affected by heat treatment. The calcination of the diatomaceous earth at 500 °C develops microporosity due to the reactions of decomposition of carbonates, dehydroxylation of silica and clays and oxidation of organic matter, which improve the surface area from 45.2 to 53.8 m2 g^{-1}. Subsequent readings from the textural analysis at temperatures between 600 and 700 °C, show a decrease in micropores that does not affect the value of the external area due to them becoming mesopores [49]. At heating above 800 °C it is observed that the external area decreases drastically possibly to mesophore sintering reactions due to the increase in the average pore size from 12.7 to 31.1 nm at 1000 °C.

3.5. Scanning Electron Microscopy (SEM)

The results of the MEB show the biogenic identity of the raw diatomaceous earth. Figure 7a shows several preserved forms of the fustules and/or skeletal structures of algae mainly from diatoms [50]. Its frustules have a cylindrical geometry of variable size and are joined together by spines that are embedded in each other to form straight and long chains (Figure 7b). In addition, impurities are observed deposited not only on the fustules, but also on other non-structural parts that obstruct their porosity. Micrographs of calcined diatomaceous

earth at 400, 800 and 1000 °C were also performed (Figure 8), in which no significant changes in its morphology are observed.

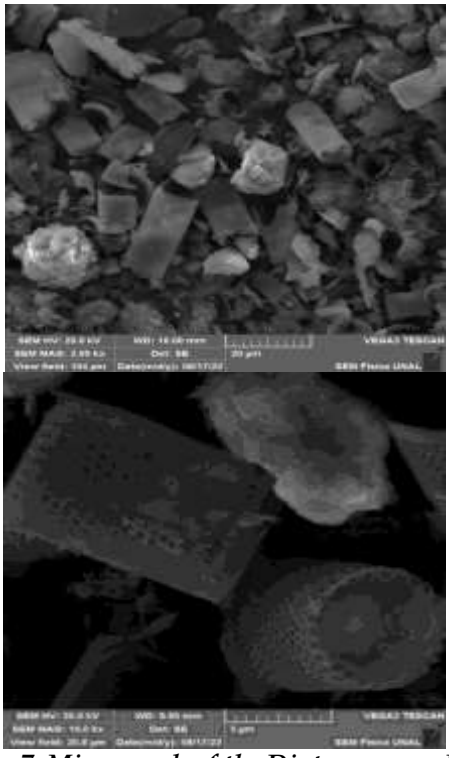

Figure 7: Micrograph of the Diatomaceous Earth with Predominant Characteristics.

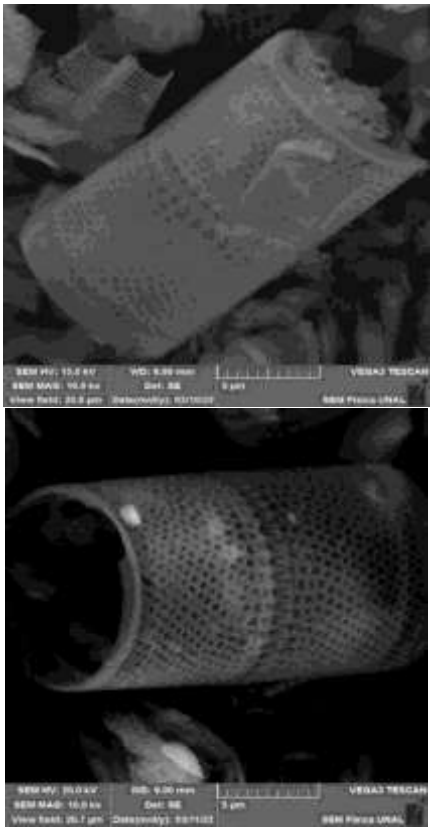

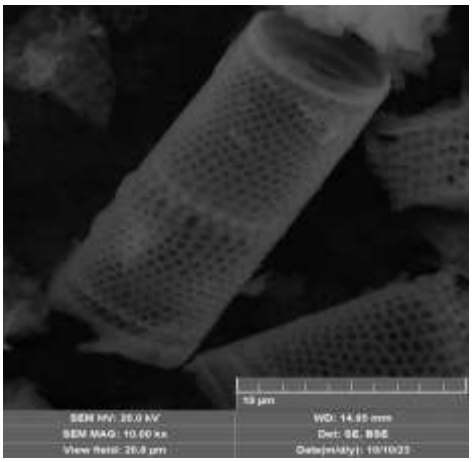

Figure 8: Micrographs of Calcined Diatomaceous Earth at 400 °C (a), 800 °C (b) and 1000 °C (c).

3.6 Adsorption Study

3.6.1. Characterization of Adsorbents after Removal of AM Dye

The infrared spectra of the Td200, CQ200 and CM200 adsorbents after removing the methylene blue dye in solution at a concentration of 200 mg dm^{-3}, are shown in Figure 9. It is observed that the characteristic bands of SiO2 and clays are maintained with respect to the raw and calcined diatomaceous earth before adsorption. The most appreciable changes occur in Td200 and CQ200 where the bands between 3770 and 3600 cm^{-1} associated with the silanol groups become more pronounced, possibly due to the formation of hydrogen bonds of the structural OH group with the N of the heterocyclic ring and the amino groups of the AM. New low-intensity absorption bands appear that indicate the presence of the AM dye and are related to vibrations of the dimethylamine group $(=N+(CH3)_2)$ at 1650 cm^{-1}, of the C=C and C=N bond of the heterocyclic ring at 1604 cm^{-1} [51], of the C-H bond at 1395 cm^{-1} and of the C-N bond at 1336 cm^{-1} [52]. In the infrared spectrum of CM200, no appreciable modifications are observed with respect to the sample calcined at 1000 °C.

With respect to textural properties, the adsorption-desorption isotherms of N2 at 77 K of the different adsorbents after removal of the AM dye remain type IV with H3 hysteresis rings as shown in Figure 10. Regarding the affectation of the specific area, it is shown in Table 2 that it decreases when comparing the values of the materials before and after adsorption. It is observed that there is a preference for filling micropores, whose area decreases by about 70% in both raw and calcined diatomaceous earth at 500 °C, compared to the area of mesophores, which decrease by about 30 and 40 % respectively.

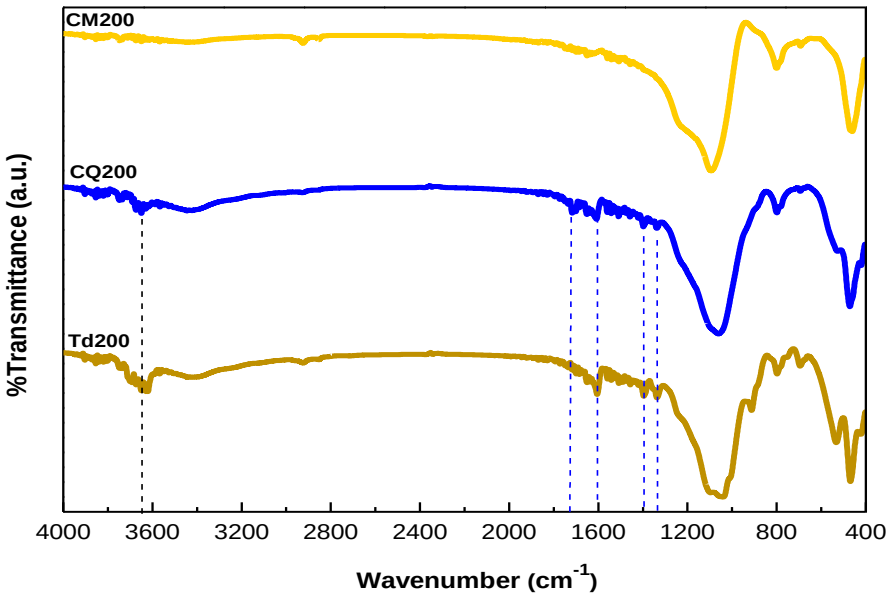

Figure 9: FTIR of Adsorbents Evaluated After Removal of the AM Dye.

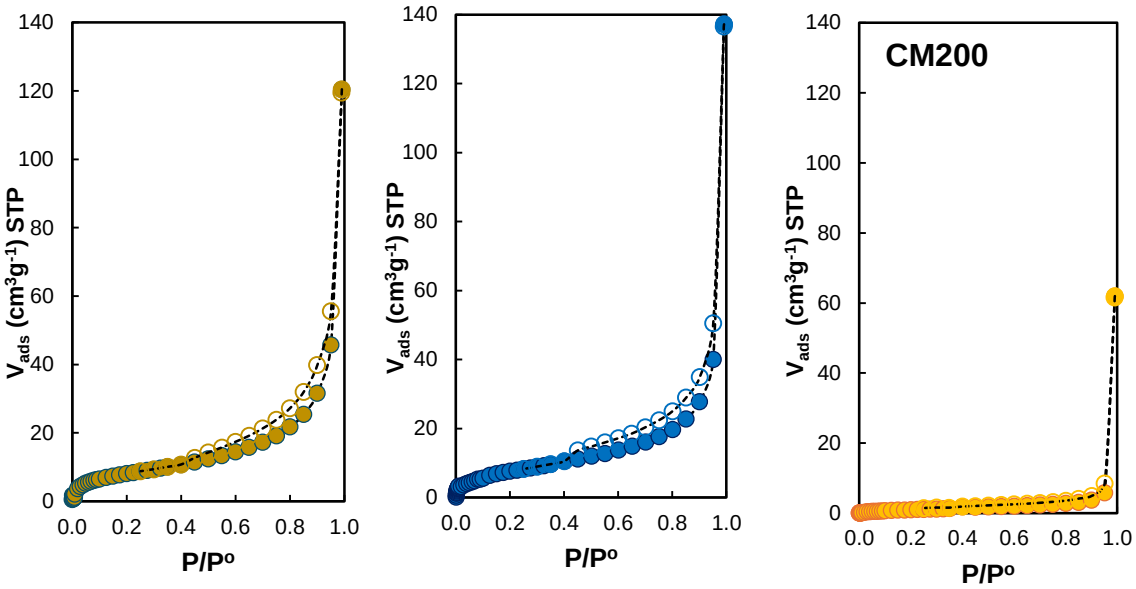

Figure 10: Adsorption-Desorption Isotherms of N□ at 77 K of Adsorbents after Removal of AM at a Concentration of 200 mg dm□³.

Table 2: Textural Properties of Adsorbents after Removal.

Adsorbent	Surface area SBET (m2 g-1)	Area External Sext (m2 g-1)	Micropore area Smicro (m2 g-1)
Td200	30.2	29.1	1.1
CQ200	29.9	27.7	2.2
CM200	4.20	4.12	0.08

3.6.2. Batch Studies

Batch adsorption experiments consist of placing a certain amount of adsorbent in contact with the solution containing the substance to be removed and keeping it in suspension by agitation for the time necessary to reach equilibrium. These results allow the percentage of removal and adsorption capacity to be calculated. In addition, fitting experimental data to isothermal models provides a measure of adsorption efficiency in removing specific adsorbates and maximum adsorption capacity.

The calculation of the removal percentage and adsorption capacity () of raw and calcined diatomaceous earth at *q*500 and 1000 °C was made from equations 9 and 10 respectively [31].

$$\% \, Remoción = \frac{(C_o - C_e)}{C_o} \text{ x } 100 \quad (9)$$

$$q_e = \frac{(C_o - C_e)V}{m} \quad (10)$$

Where is the volume of the solution used in dmV^3 and is the mass, in grams, of adsorbent used$m$. The effect of the initial concentration of methylene blue dye in the range between 20.0 and 200.0 mg dm-3 at 23 °C is shown in Figure 11.

Figure 11a shows that the percentage of AM dye removal decreases with increasing initial concentration for all adsorbents evaluated. At low concentrations of methylene blue dye, some active adsorption sites are occupied and after reaching equilibrium, others are available, achieving high removal percentages for Td and CQ. In the case of the CM adsorbent, the removal of the silanol groups and the decrease in the specific area after calcination at 1000 °C (Figure 4), limits the adsorption process to removal percentages of 44%.

On the other hand, Figure 11b shows how the adsorption capacity increases with the initial concentration of the AM dye. This behavior is due to the fact that, initially, the adsorption sites are occupied with molecules of the AM dye and, as the initial concentration increases, the availability of these sites decreases, reaching the saturation of the adsorbent, which is graphically observed when the adsorption capacity remains constant.

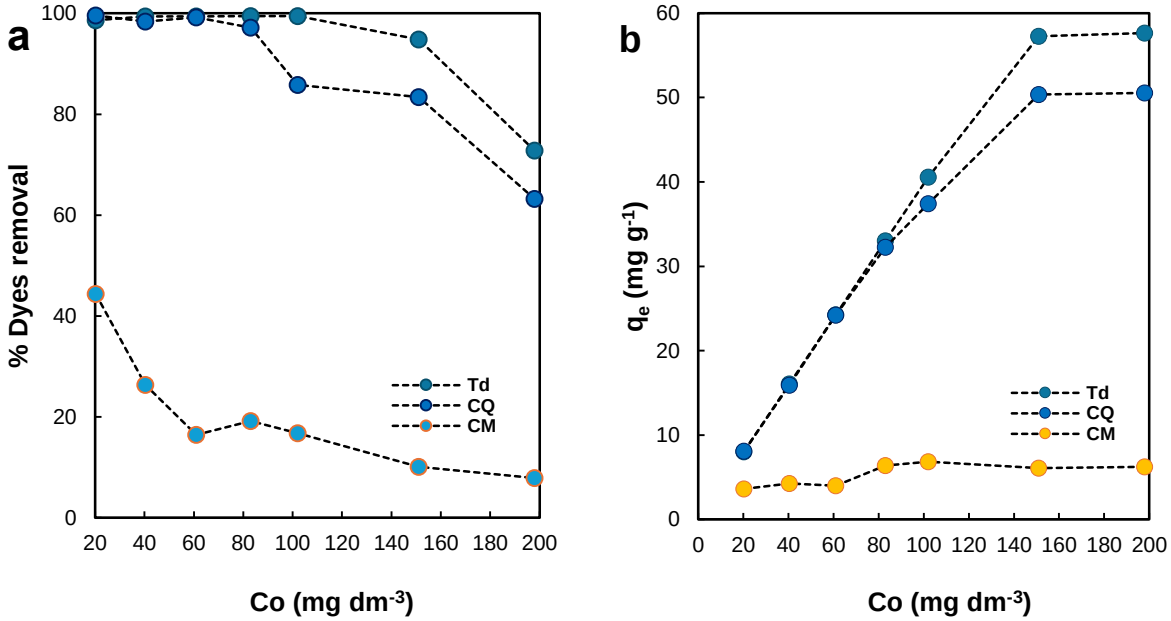

Figure 11: Effect of the Initial Concentration on (a) the Removal Percentage and (b) the Adsorption Capacity.

3.6.2.1 Adsorption Isotherms

Mathematical models of isotherms relate the adsorption capacity and concentration of the substance to be removed and which remains in solution when equilibrium is reached at a constant temperature. The results of the batch study were fitted to two models of isotherms: Langmuir and Freundlich. The Langmuir model assumes that equilibrium is reached when a monolayer of adsorbate molecules saturates the adsorbent at identical active sites and that there is no interaction between the adsorbed molecules [31]. The values of y in equation 2 were calculated from the slope and the intercept when plotting versus (Figure 12).$K_L q_{max} \frac{C_e}{q_e} C_e$

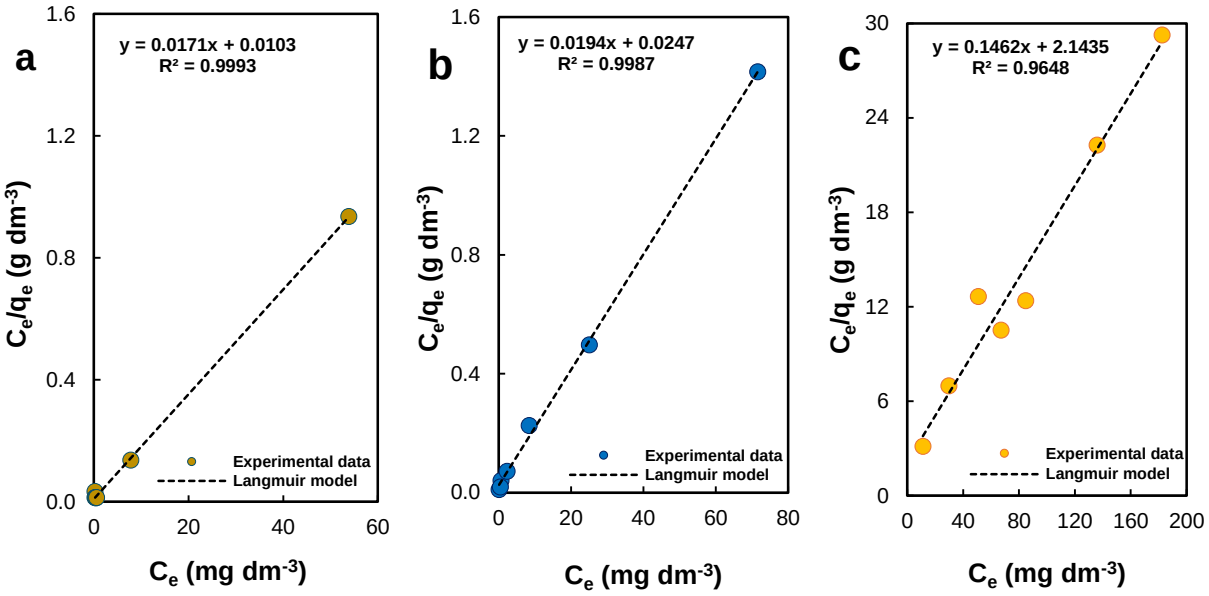

Figure 12: Methylene Blue Adsorption Equilibrium Data Fitted to the Langmuir Isotherm Model: a) Td, b) CQ, and c) CM.

The Freundlich model assumes that the surface of the adsorbent is heterogeneous and that the adsorption sites have different affinities. First, the positions of greatest affinity are occupied and, subsequently, the rest are occupied [31]. The values of y in equation 3 were calculated from the slope and the intercept when plotting versus (Figure 13). $K_F nlnq_e lnC_e$

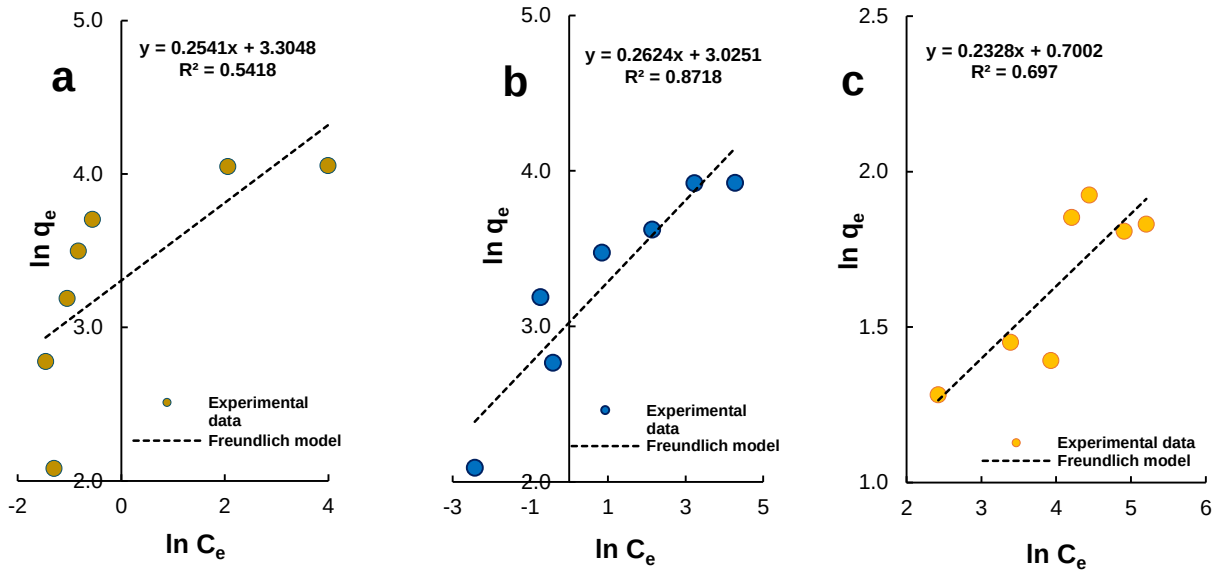

Figure 13: Methylene Blue Adsorption Equilibrium Data Fitted to the Freundlich Isotherm Model: a) Td, b) CQ, and c) CM.

The values of the constants of both models, together with the coefficients of determination, are shown in Table 3. These indicate that the Langmuir isotherm model presents the best fit of the experimental data of the study per lot, with values greater than 0.96. This suggests that the adsorption of methylene blue dye on the surface of the crude and calcined diatomaceous earth is characterized by a monolayer coating. R^2 The maximum adsorption capacity was obtained by crude diatomaceous earth with a value of 58.5 mg g-1, followed by calcined at 500 °C, with 51.5 mg g-1. These results show the

influence of texture properties on adsorption processes, as well as the presence of silica silanol groups, which allow it to establish hydrogen bonds with the N of the heterocyclic ring and the amino groups of the AM dye. The significant decrease in both factors in the CM sample justifies the low capacity determined by the Langmuir model. The values of , obtained from the Freundlich model, are all greater than 1, which indicates that the adsorption is favorable for all the conditions studied.n

Table 3: Langmuir and Freundlich Isothermal Constants.

Adsorbent	Langmuir Isotherm			Freundlich Isotherm		
	q_{max} (mg g^{-1})	K_L (dm3 mg^{-1})	R^2	K_F	n	R^2
Td	58.5	1.66	0.99	27.2	3.9	0.54
CQ	51.5	0.78	0.99	20.6	3.8	0.87
CM	6.84	0.07	0.96	2.0	4.3	0.69

3.6.3. Column Studies

For the column study, crude and calcined diatomaceous earth at 500 °C were selected as adsorbent material, since they presented the best adsorption capacities in the batch study. In addition, the rupture time was established as the time it takes for the bed to reach 10% of the initial concentration, that is, when $\frac{C}{C_o}$= 0.1, obtained from Figure 14, known as the rupture curve that results from plotting the relationship as a function of time. This figure shows the behavior followed by the removal of methylene blue dye for each of the adsorbents evaluated at three heights (1.0, 1.5 and 2.0 cm), with an initial concentration of 20.0 mg dm-3$\frac{C}{C_o}$ and a volumetric flow of 0.5 cm3 $^{min-1}$. The values of the adsorption capacity at the breaking point (), calculated according to equation 3, are summarized in Table 4.q_b

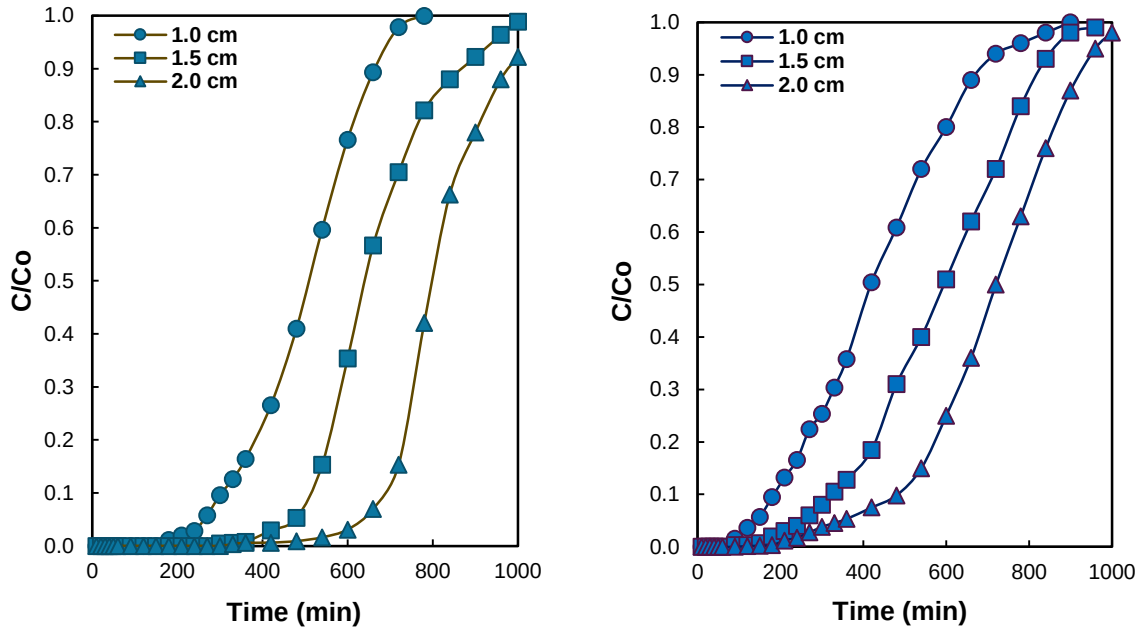

Figure 14: Breakdown Curves for Adsorption of Violet Crystal Dye in a Column Packed with (a) Td and (b) CQ.

All of the breakdown curves shown in Figure 14 have the same behavior: initially, the bottom of the bed removes the methylene blue dye, so the fluid exiting the column is virtually dye-free. As the volume of fluid passing through the column increases, the mass transfer zone (MTZ) shifts and the concentration of the dye at the outlet increases over time. The bed is completely saturated when the concentration of the dye at the outlet is the same as at the inlet, i.e. when the ZTM has left the column.

Table 4 shows that the highest adsorption capacity achieved in column was 25.2 mg $^{g-1}$, using raw diatomaceous earth as an adsorbent, at a height of 2.0 cm. This result is lower than the value obtained in the batch study (58.5 mg $^{g-1}$) calculated from the Langmuir isotherm. This difference is due to the fact

that, in the batch study, both raw and calcined diatomaceous earth at 500 °C are under permanent agitation for a longer time of contact with the same solution, which favors the mass transfer of the methylene blue dye, while in the column study there is continuous contact with fresh streams. In both studies, raw diatomaceous earth presents the best removal results. In addition, it is observed that by increasing the bed height from 1.0 to 2.0 cm for the two adsorbents, more active sites are available, since the surface area increases, so all breakdown times are increased, as well as the adsorption capacity.

Table 4: Adsorption capacity in column a = 20.3 mg dm-3C_o y = 0.5 cm$Q_v$$^{3\ min-1}$.

Adsorbent	Column Height (cm)	Breakout Time (min)	Adsorbent bed mass (g)	Column adsorption capacity (mg g^{-1})
Td	1.0	304	0.1453	21.2
	1.5	500	0.2142	23.7
	2.0	696	0.2805	25.2
CQ	1.0	188	0.1116	17.1
	1.5	326	0.1685	19.6
	2.0	482	0.2308	21.2

3.6.3.1 Application of the Bed Height Service Time (BDST) Model

The experimental results of the service times of the columns packed with raw and calcined diatomaceous earth at 500 °C at different heights for the removal of methylene blue dye were adjusted to the BDST model. Figures 15a and 16a show the representation of some of the isoremoval lines () of the BDST model. From the values of the slope and intercept at the origin of each of the trend lines, y (Table 5) were obtained.$\frac{C}{C_o} N_o\ K$

The values of the coefficients of determination of raw diatomaceous earth show a better fit to the BDST model ($R2 > 0.98$), than those of calcined at 500 °C. By replacing N_o and in equation 4 for the selected break time (0.1), $K\ \frac{C}{C_o} =\ C_o$ = 20.0 mg dm-3, = 2.55 cm $U^{\text{min-1}}$ and 0.1,$\frac{C}{C_o}$ = the relationship between the break time and bed height is established. Equations 11 and 12 summarize these calculations for Td and CQ respectively.

$$t = 374Z - 64 \quad (11)$$
$$t = 294Z - 109 \quad (12)$$

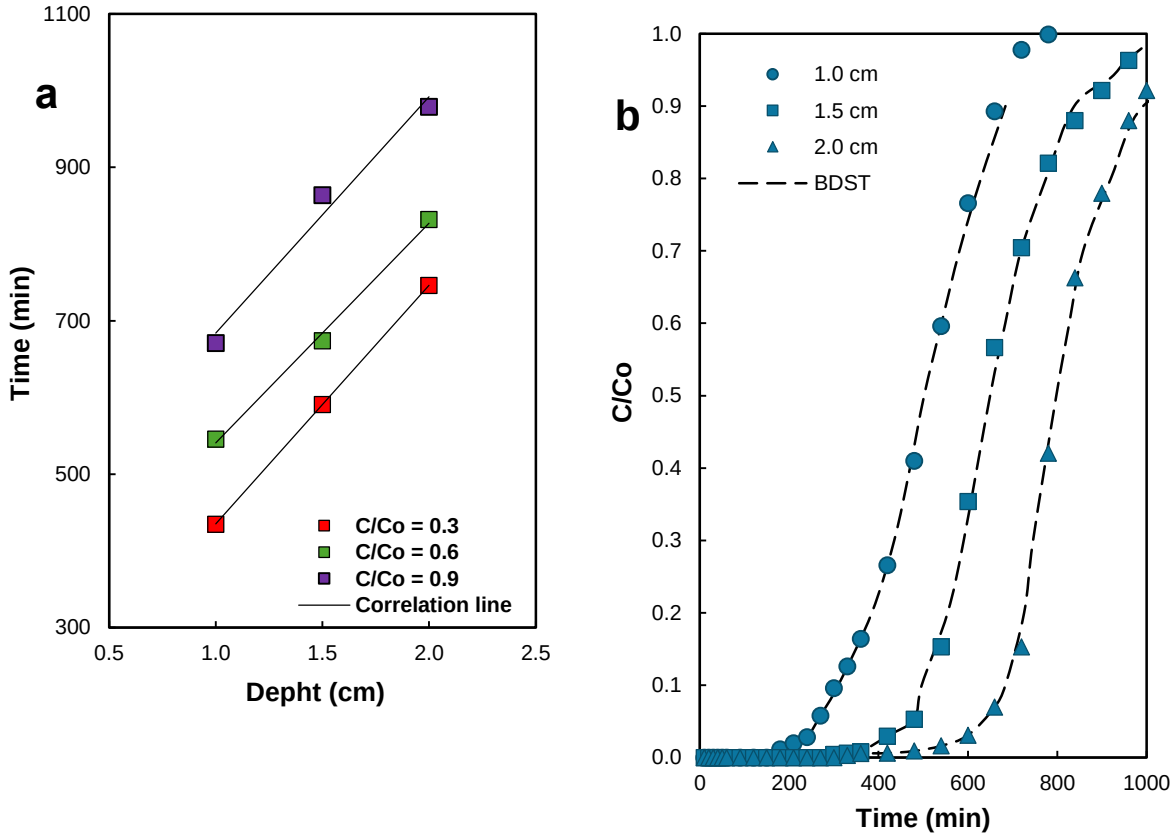

Figure 15: Raw Diatomaceous Earth: a) Isoremoval Lines at Different Heights, and b) Experimental Data Adjusted to the BDST Model.

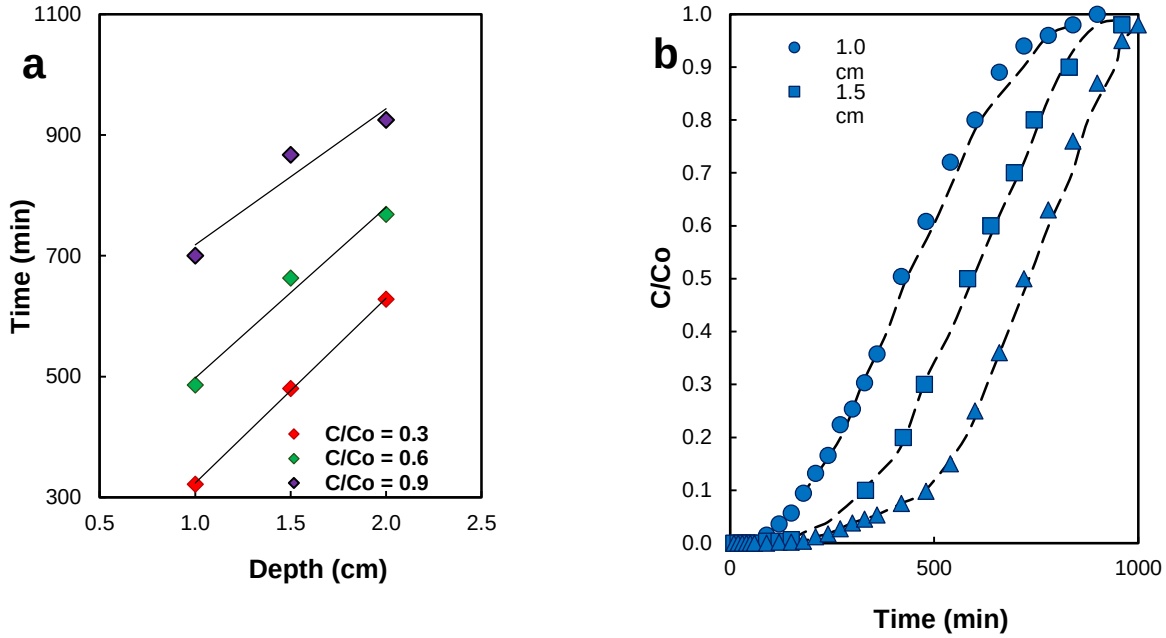

Figure 16. Diatomaceous Earth Calcined at 500 °C: a) Isoremoval Lines at Different Heights, and b) Experimental Data Adjusted to the BDST Model.

Table 5: BDST Model Parameters.

Adsorbent	$\frac{C}{C_o}$	N_o (mg dm^{-3})	K (dm3 min^{-1} mg^{-1})	$R2$
Td	0.1	19360	1.7 x 10^{-3}	0.99
	0.6	14805	1.0 x 10^{-4}	0.99
	0.9	15944	3.0 x 10^{-4}	0.98
CQ	0.1	15219	1.0 x 10^{-3}	0.99
	0.6	14624	1.0 x 10^{-3}	0.97
	0.9	11647	1.2 x 10^{-3}	0.93

Table 6 compares the breakdown time values obtained experimentally and those calculated from equations 11 and 12. The BDST model satisfactorily fits the experimental results for all the heights evaluated. This indicates that for this study the intraparticle diffusion and the external mass resistance are not significant as proposed by the BDST model. Figures 15b and 16b show the graphical comparison of experimental and adjusted breakdown curves.

Table 6: Comparison between Experimental and Calculated Breakdown Times of the BDST Model.

Adsorbent	Bed height (cm)	Experimental breakout time (min)	Calculated breakout time (min)
Td	1.0	304	310
	1.5	500	497
	2.0	696	684
CQ	1.0	188	185
	1.5	326	332
	2.0	482	479

4. CONCLUSION

The experimental methodology developed in this research consisted of determining the textural, crystallographic and morphological modifications that occur during the heat treatment of a sample of diatomaceous earth from the municipality of Chivatá (Boyacá, Colombia) and evaluating its capacity as an adsorbent material in the elimination of methylene blue dye in aqueous solution by batch and continuous flow processes at different heights of the bed. The results obtained allow the following conclusions to be formulated:

- The conservation of the frustules, the persistence of mesoporosity and the maintenance of the signals corresponding to opal-A and quartz, after calcination at temperatures between 200 and 1000°C, show the thermal stability of the diatomaceous earth.
- With respect to the batch study, the percentage of methylene blue dye removal decreases and the adsorption capacity increases with increasing initial concentration. Experimental data from crude and calcined diatomaceous earth at 500 and 1000 °C show a good fit to the Langmuir isotherm model with determination factors greater than 0.96. The maximum adsorption capacity was obtained by crude diatomaceous earth, with a value of 58.5 mg g-1, followed by calcined at 500 °C, with 51.5 mg g-1.

- In the column study, the maximum adsorption capacity was 25.2 mg g-1 using crude diatomaceous earth as an adsorbent, at a height of 2.0 cm, volumetric flow of 0.5 cm3 min-1 and an initial concentration of 20.3 mg dm-3. The breakdown curves obtained show that both the breakdown time and the adsorption capacity of Td and CQ increase with increasing bed height. The bed height service time (BDST) model fits satisfactorily with the experimental results for all the heights evaluated.

Acknowledgements: The authors of this article are grateful for the collaboration of the Laboratories of Fuels and Energy and, of Heterogeneous Catalysis, Physicochemical Applications of the Solid State, of the National University of Colombia, the Chemistry Laboratory of the Autonomous University of the Caribbean and the School of Military Engineers.

Conflict of Interest: The authors did not declare any conflict of interest.

REFERENCES

[1] Yuan P., Liu D., Tan D. Y., Liu K. K., Yu H. G., Zhong Y. H., Yuan A. H., Yu W. B., He H. P. Surface silylation of mesoporous/macroporous diatomite (diatomaceous earth) and its function in Cu(II) adsorption: The effects of heating pretreatment. Micropor. Mesopor. Mat. 2013; 170:9–19. https://doi.org/10.1016/j.micromeso.2012.11.030

[2] Lamastra F. R., Mori S., Cherubini V., Scarselli M., Nanni F. A new green methodology for surface modification of diatomite filler in elastomers. Mater. Chem. Phys. 2017; 194:253–260. https://doi.org/10.1016/j.matchemphys.2017.03.050

[3] Zhang J., Ping Q., Niu M., Shi H., Li N. Kinetics and equilibrium studies from the methylene blue adsorption on diatomite treated with sodium hydroxide. Appl. Clay. Sci. 2013; 83–84:12–6. http://dx.doi.org/10.1016/j.clay.2013.08.008

[4] Phogat S., Saxena A., Kapoor N., Aggarwal C., Tiwari A. Diatom mediated smart drug delivery system. J. Drug Deliv. Technol. 2021; 63:102433. http://dx.doi.org/10.1016/j.jddst.2021.102433

[5] Hildebrand M., Lerch S. J. L., Shrestha R. P. Understanding Diatom Cell Wall Silicification—Moving Forward. Front. Mar. Sci. 2018; 5:125. http://dx.doi.org/10.3389/fmars.2018.00125

[6] Poulsen N., Kröger N. Silica Morphogenesis by Alternative Processing of Silaffins in the Diatom Thalassiosira pseudonana. J. Biol. Chem. 2004; 279(41):42993–9. http://dx.doi.org/10.1074/jbc.m407734200

[7] Danil de Namor A. F., El Gamouz A., Frangie S., Martinez V., Valiente L., Webb O. A. Turning the volume down on heavy metals using tuned diatomite. A review of diatomite and modified diatomite for the extraction of heavy metals from water. J. Hazard. Mater. 2012; 241–242:14–31. http://dx.doi.org/10.1016/j.jhazmat.2012.09.030

[8] Kokunešoski M., Šaponjić A., Stanković M., Majstorović J., Egelja A., Ilić S., Matović B. Effect of boric acid on the porosity of clay and diatomite monoliths. Ceram. Int. 2016; 42(5):6383–90. http://dx.doi.org/10.1016/j.ceramint.2016.01.034

[9] Sriram G., Kigga M., Uthappa U. T., Rego R. M., Thendral V., Kumeria T., Jung H. Y., Kurkuri M. D. Naturally available diatomite and their surface modification for the removal of hazardous dye and metal ions: A review. Adv. Colloid Interface Sci. 2020; 282:102198. http://dx.doi.org/10.1016/j.cis.2020.102198

[10] Yan S., Huo W., Yang J., Zhang X., Wang Q., Wang L., Pan Y., Huang Y. Green synthesis and influence of calcined temperature on the formation of novel porous diatomite microspheres for efficient adsorption of dyes. Powder Technol. 2018; 329:260–9. http://dx.doi.org/10.1016/j.powtec.2018.01.090

[11] Martinovic S., Vlahovic M., Boljanac T., Pavlovic L. Preparation of filter aids based on diatomites. Int. J. Miner. Process. 2006; 80(2–4):255–60. http://dx.doi.org/10.1016/j.minpro.2006.05.006

[12] Kouzu M., Hidaka J. Suke. Transesterification of vegetable oil into biodiesel catalyzed by CaO: A review. Fuel 2012; 93:1–12. http://dx.doi.org/10.1016/j.fuel.2011.09.015

[13] Modiba E., Enweremadu C., Rutto H. Production of biodiesel from waste vegetable oil using impregnated diatomite as heterogeneous catalyst. Chin. J. Chem. Eng. 2015; 23(1):281–9. http://dx.doi.org/10.1016/j.cjche.2014.10.017

[14] Rabie A. M., Shaban M., Abukhadra M. R., Hosny R., Ahmed S. A., Negm N. A. Diatomite supported by CaO/MgO nanocomposite as heterogeneous catalyst for biodiesel production from waste cooking oil. J. Mol. Liq. 2019; 279:224–31. http://dx.doi.org/10.1016/j.molliq.2019.01.096
[15] Shan R., Zhao C., Yuan H., Wang S., Wang Y. Transesterification of vegetable oil using stable natural diatomite-supported catalyst. Energy Convers. Manag. 2017; 138:547–55. http://dx.doi.org/10.1016/j.enconman.2017.02.028
[16] Akti F. Photocatalytic degradation of remazol yellow using polyaniline–doped tin oxide hybrid photocatalysts with diatomite support. Appl. Surf. Sci. 2018; 455:931–9. http://dx.doi.org/10.1016/j.apsusc.2018.06.019
[17] Dang T. D., Banerjee A. N., Tran Q. T., Roy S. Fast degradation of dyes in water using manganese-oxide-coated diatomite for environmental remediation. J. Phys. Chem. Solids 2016; 98:50–8. http://dx.doi.org/10.1016/j.jpcs.2016.06.006
[18] Delasoie J., Zobi F. Natural Diatom Biosilica as Microshuttles in Drug Delivery Systems. Pharmaceutics 2019; 11(10):537. http://dx.doi.org/10.3390/pharmaceutics11100537
[19] Ahmadi Z., Esmaeili J., Kasaei J., Hajialioghli R. Properties of sustainable cement mortars containing high volume of raw diatomite. Sust. Mater. Technol. 2018; 16:47–53. http://dx.doi.org/10.1016/j.susmat.2018.05.001
[20] Hassan H. S., Abdel-Gawwad H. A., Vásquez-García S. R., Israde-Alcántara I., Flores-Ramírez N., Rico J. L., Mohammed M. S. Cleaner production of one-part white geopolymer cement using pre-treated wood biomass ash and diatomite. J. Clean. Prod. 2019; 209:1420–8. http://dx.doi.org/10.1016/j.jclepro.2018.11.137
[21] Taoukil D., El Meski Y., Lahlaouti M. lhassane, Djedjig R., El Bouardi A. Effect of the use of diatomite as partial replacement of sand on thermal and mechanical properties of mortars. J. Build. Eng. 2021; 42:103038. http://dx.doi.org/10.1016/j.jobe.2021.103038
[22] Yılmaz B., Ediz N. The use of raw and calcined diatomite in cement production. Cem. Concr. Compos. 2008; 30(3):202–11. http://dx.doi.org/10.1016/j.cemconcomp.2007.08.003
[23] Jain R., Dhali S., Nigam H., Malik A., Malik H. K., Satyakam R. Recovery of diatom bio-silica using chemical, thermal, and plasma treatment. Bioresour. Technol. Rep. 2022; 18:101035. http://dx.doi.org/10.1016/j.biteb.2022.101035
[24] Alyosef H. A., Ibrahim S., Welscher J., Inayat A., Eilert A., Denecke R., Schwieger W., Münster T., Kloess G., Einicke W. D. Effect of acid treatment on the chemical composition and the structure of Egyptian diatomite. Int. J. Miner. Metall. Mater. 2014; 132:17–25. http://dx.doi.org/10.1016/j.minpro.2014.09.001
[25] Du F., Li J., Li X., Zhang Z. Improvement of iron removal from silica sand using ultrasound-assisted oxalic acid. Ultrason. Sonochem. 2011; 18(1):89–93. http://dx.doi.org/10.1016/j.ultsonch.2010.07.006
[26] Lee S. O., Tran T., Jung B. H., Kim S. J., Kim M. J. Dissolution of iron oxide using oxalic acid. Hydrometallurgy 2007; 87(3–4):91–9. http://dx.doi.org/10.1016/j.hydromet.2007.02.005
[27] Khraisheh M. A. M., Al-Ghouti M. A., Allen S. J., Ahmad M. N. Effect of OH and silanol groups in the removal of dyes from aqueous solution using diatomite. Water. Res. 2005; 39(5):922–32. http://dx.doi.org/10.1016/j.watres.2004.12.008
[28] Al-Qodah Z., Lafi W. K., Al-Anber Z., Al-Shannag M., Harahsheh A. Adsorption of methylene blue by acid and heat treated diatomaceous silica. Desalination 2007; 217(1–3):212–24. http://dx.doi.org/10.1016/j.desal.2007.03.003
[29] Zhang J., Ping Q., Niu M., Shi H., Li N. Kinetics and equilibrium studies from the methylene blue adsorption on diatomite treated with sodium hydroxide. Appl. Clay. Sci. 2013; 83–84:12–6. http://dx.doi.org/10.1016/j.clay.2013.08.008
[30] Rehman M. U., Taj M. B., Carabineiro S. A. C. Biogenic adsorbents for removal of drugs and dyes: A comprehensive review on properties, modification and applications. Chemosphere 2023; 338:139477. http://dx.doi.org/10.1016/j.chemosphere.2023.139477
[31] Cely-Bautista M. M., Cardozo-Arrieta B. M., Jaramillo-Colpas J. E., Moreno-Aldana L. C., Valencia-Ríos J. S., Castellar-Ortega G. C. Evaluation of diatomaceous earth in the removal of crystal violet dye in solution. J. Appl. Res. Technol. 2022; 20(4):387–98. http://dx.doi.org/10.22201/icat.24486736e.2022.20.4.1524
[32] Bohart G. S., Adams E. Q. Some aspects of the behavior of charcoal with respect to chlorine 1. J. Am. Chem. Soc. 1920; 42(3):523–44. http://dx.doi.org/10.1021/ja01448a018

[33] Taty-Costodes V. C., Fauduet H., Porte C., Ho Y. S. Removal of lead (II) ions from synthetic and real effluents using immobilized Pinus sylvestris sawdust: Adsorption on a fixed-bed column. J. Hazard. Mater. 2005; 123(1–3):135–44. http://dx.doi.org/10.1016/j.jhazmat.2005.03.032
[34] Awadh S. M., Yaseen Z. M. Investigation of silica polymorphs stratified in siliceous geode using FTIR and XRD methods. Mater. Chem. Phys. 2019; 228:45–50. http://dx.doi.org/10.1016/j.matchemphys.2019.02.048
[35] Reka A. A., Pavlovski B., Fazlija E., Berisha A., Pacarizi M., Daghmehchi M., Jovanoski G., Makreski P., Oral A. Diatomaceous Earth: Characterization, thermal modification, and application. Open Chem. 2021; 19(1):451–61. http://dx.doi.org/10.1515/chem-2020-0049
[36] Labidi N. S., Mechati B. Adsorption mechanism of basic blue-9 onto quartz mineral: kinetics, isotherms and thermodynamic. Mater. Res. Express 2022; 9(11):115501. http://dx.doi.org/10.1088/2053-1591/ac9cb7
[37] Pasabeyoglu P., Moumin G., de Oliveira L., Roeb M., Akata B. Solarization of the zeolite production: Calcination of kaolin as proof-of-concept. J. Clean Prod. 2023; 414:137611. http://dx.doi.org/10.1016/j.jclepro.2023.137611
[38] Frost R. L., Horváth E., Makó É., Kristóf J., Rédey Á. Slow transformation of mechanically dehydroxylated kaolinite to kaolinite—an aged mechanochemically activated formamide-intercalated kaolinite study. Thermochim. Acta 2003; 408(1–2):103–13. http://dx.doi.org/10.1016/s0040-6031(03)00316-2
[39] Ptáček P., Frajkorová F., Šoukal F., Opravil T. Kinetics and mechanism of three stages of thermal transformation of kaolinite to metakaolinite. Powder Technol. 2014; 264:439–45. http://dx.doi.org/10.1016/j.powtec.2014.05.047
[40] İssi A. Estimation of ancient firing technique by the characterization of semi-fused Hellenistic potsherds from Harabebezikan/Turkey. Ceram. Inter. 2012; 38(3):2375–80. http://dx.doi.org/10.1016/j.ceramint.2011.11.002
[41] Vásquez-Torres O. O., Cabrera-Poloche F. D., Tobón J. I. Performance of Low-Grade Calcined Clays as Supplementary Cementitious Material in Relation to their Geological Characteristics. Clays Clay Miner. 2022; 70(2):233–51. http://dx.doi.org/10.1007/s42860-022-00184-7
[42] Janićijević J., Krajišnik D., Čalija B., Dobričić V., Daković A., Krstić J., Marković M., Milić J. Inorganically modified diatomite as a potential prolonged-release drug carrier. Mater. Sci. Eng. C 2014; 42:412–20. http://dx.doi.org/10.1016/j.msec.2014.05.052
[43] Inchaurrondo N., Font J., Ramos C. P., Haure P. Natural diatomites: Efficient green catalyst for Fenton-like oxidation of Orange II. Appl. Catal. B-Environ. 2016; 181:481–94. http://dx.doi.org/10.1016/j.apcatb.2015.08.022
[44] Ma S. C., Wang Z. G., Zhang J. L., Sun D. H., Liu G. X. Detection analysis of surface hydroxyl active sites and simulation calculation of the surface dissociation constants of aqueous diatomite suspensions. Appl. Surf. Sci. 2015; 327:453–61. http://dx.doi.org/10.1016/j.apsusc.2014.12.006
[45] Tatzber M., Stemmer M., Spiegel H., Katzlberger C., Haberhauer G., Mentler A., Gerzabek M. H. FTIR-spectroscopic characterization of humic acids and humin fractions obtained by advanced NaOH, Na4P2O7, and Na2CO3 extraction procedures. J. Plant Nut. Soil Sci. 2007; 170(4):522–9. http://dx.doi.org/10.1002/jpln.200622082
[46] Reka A., Kosanovic D., Ademi E., Aggrey P., Berisha A., Pavlovski B., Jovanovski G., Rexhepi B., Jashari A., Makeski P. Fabrication of ceramic monoliths from diatomaceous earth: effects of calcination temperature on silica phase transformation. Sci. Sinter. 2022; 54(4):495–506. http://dx.doi.org/10.2298/sos2204495r
[47] Mendioroz S., Belzunce M. J., Pajares J. A. Thermogravimetric study of diatomites. J. Therm. Anal. 1989; 35(7):2097–104. http://dx.doi.org/10.1007/bf01911874
[48] Cychosz K. A., Thommes M. Progress in the Physisorption Characterization of Nanoporous Gas Storage Materials. Engineering 2018; 4(4):559–66. http://dx.doi.org/10.1016/j.eng.2018.06.001
[49] Agámez Y., Oviedo L., Navarro U., Centeno M., Odriozola J. Modifications of the textural and structural properties of a USY zeolite and its mixtures with "kaolin clay" and chlorhydrol as a consequence of hydrothermal treatment. Rev. Colomb. Quim. 2006; 35(1):7–17. https://repositorio.unal.edu.co/handle/unal/22297
[50] Goren R., Baykara T., Marsoglu M. Effects of purification and heat treatment on pore structure and composition of diatomite. Br. Ceram. Trans. 2002; 101(4):177–80. http://dx.doi.org/10.1179/096797802225003361

[51] Villota-Enríquez M. D., Rodríguez-Páez J. E. Bio-silica production from rice husk for environmental remediation: Removal of methylene blue from aqueous solutions. Mater. Chem. Phys. 2023; 301:127671. http://dx.doi.org/10.1016/j.matchemphys.2023.127671

[52] Li Z., Wang C. J., Jiang W. T. Intercalation of Methylene Blue in a High-Charge Calcium Montmorillonite — An Indication of Surface Charge Determination. Adsorp. Sci. Technol. 2010; 28(4):297–312. http://dx.doi.org/10.1260/0263-6174.28.4.297